Journal of Alloys and Compounds 868 (2021) 159253

Contents lists available at ScienceDirect

Journal of Alloys and Compounds

journal homepage: www.elsevier.com/locate/jalcom

Routes to develop a [S]/([S]+[Se]) gradient in wide band-gap $Cu_2ZnGe(S,Se)_4$ thin-film solar cells

Andrea Ruiz-Perona[a], Galina Gurieva[b], Michael Sun[a,1], Tim Kodalle[c], Yudania Sánchez[d], Maarja Grossberg[e], José Manuel Merino[a], Susan Schorr[b,f], Máximo León[a], Raquel Caballero[a,*]

[a] Universidad Autónoma de Madrid, Departamento de Física Aplicada, C/ Francisco Tomás y Valiente 7, Madrid 28049, Spain
[b] Helmholtz Zentrum Berlin für Materialien und Energie, Hahn-Meitner Platz 1, Berlin 14109, Germany
[c] PVcomB, Helmholtz Zentrum Berlin für Materialien und Energie, Schwarzschildstrasse 3, Berlin 12489 Germany
[d] IREC, Catalonia Institute for Energy Research, C/ Jardins de les Dones de Negre 1, Barcelona 08930, Spain
[e] Tallinn University of Technology, Ehitajate Tee 5, Tallinn 19086, Estonia
[f] Freie Universitaet Berlin, Department of Geosciences, Malteserstrasse 74-100, Berlin 12249, Germany

ARTICLE INFO

Article history:
Received 3 November 2020
Received in revised form 29 January 2021
Accepted 17 February 2021
Available online 19 February 2021

Keywords:
Kesterite
Solar cells
Sodium
Selenium capping layer
Sulphur-gradient
Wide band gap energy

ABSTRACT

Wide band-gap kesterite-based solar cells are very attractive to be used for tandem devices as well as for semi-transparent photovoltaic cells. Here, $Cu_2ZnGe(S,Se)_4$ (CZGSSe) thin films have been grown by sulfurization of co-evaporated $Cu_2ZnGeSe_4$. The influence of a NaF precursor layer and of a Se capping film on CZGSSe absorbers and solar cells has been investigated. It has been found that the distribution of [S]/([S]+[Se]) through the CZGSSe absorber layer is strongly dependent on the Na content. Na promotes the diffusion of S towards the bulk of the absorber layer. Thicker NaF layers >6 nm lead to a higher S content in the bulk of the absorber layer, but to a decreased accumulation of sulphur at the surface, as detected by GIXRD, GD-OES, and Raman spectroscopy measurements. A relationship between J_{sc}, *FF* and Na-content supplied was found; higher Na content resulted in improved solar cell efficiencies. It has also been possible to modify the [S]/([S]+[Se])-gradient throughout the CZGSSe film by the absence of the Se capping layer, achieving devices with 2.7% performance and E_g = 2.0 eV. This work reveals two ways to control the [S]/([S]+[Se]) depth-profile to produce wide band gap CZGSSe absorber layers for efficient solar cells.

1. Introduction

In the last years, kesterite-type $Cu_2ZnSn(S,Se)_4$ (CZTSSe) has been shown as a promising material to be used as absorber for thin-film solar cells. This material presents a high optical absorption coefficient, a tuneable band gap energy from 1.0 eV ($Cu_2ZnSnSe_4$) to 1.6 eV (Cu_2ZnSnS_4), and a *p*-type conductivity. Furthermore, CZTSSe is composed of earth-abundant elements of low toxicity, making this material more attractive. However, the record efficiency of CZTSSe-based solar cells is still of η = 12.6% [1,2], very far from that obtained by $Cu(In,Ga)Se_2$-based photovoltaic devices [3]. Many works have reported that the large V_{OC}-deficit, which can be defined as $E_g/q - V_{OC}$, is the main limitation of this technology [2,4,5]. Different attempts have been carried out to find a way for the reduction of the recombinational losses that are identified as the main source of the V_{OC}-deficit. The partial substitution of Sn with Ge has led to a reduced V_{OC}-deficit, which was suggested to be due to the suppression of Sn-related defects [4]. An efficiency of 12.3% was achieved for $Cu_2Zn(Sn,Ge)Se_4$ (CZTGSe)-based solar cells with [Ge]/([Sn]+[Ge]) atomic ratio of 0.22 and E_g = 1.1 eV [5]. The increase of the Ge concentration in the kesterite structure resulted in a higher band gap energy, around 1.4 eV for $Cu_2ZnGeSe_4$ (CZGSe) [6] and 2.25 eV for Cu_2ZnGeS_4 (CZGS) [7], but also in a lower device performance [8,9]. This decreased solar cell efficiency has been related to the formation of a deep donor defect [8,9]. Very recently, the emerging trend of Ge for Sn substitution has been shown as a successful strategy to improve the open circuit voltage, achieving 8.5% efficiency for CZGSe-based solar cells [10].

On the other hand, the observed positive effect of some alkaline elements on kesterite-type thin films has been the goal of some laboratories to enhance the efficiency of kesterite solar cells [11]. Up to now, Na and Li are the most promising alkalis for that [12]. A

* Corresponding author.
E-mail address: raquel.caballero@uam.es (R. Caballero).
[1] Present address: Universidad de Alcalá, Carretera Madrid-Barcelona Km. 33.6, Alcalá de Henares 28871, Spain.

https://doi.org/10.1016/j.jallcom.2021.159253
0925-8388/

12.2% efficiency (active area) was achieved by introducing Li in the kesterite material, as reported by Cabas-Vidani et al. [13]. Na is the most investigated alkaline element, enabling larger kesterite grain sizes and increasing the carrier concentration [11]. In addition, an influence of Na on the in-depth distribution of elements through the absorber layer [14], as well as on the incorporation of S into CZTSe lattice has been detected [15]. Recently, the promotion of Ge in CZTSe via Na addition has been shown, demonstrating the role of Na also in indirectly tuning the band gap energy of kesterite semiconductors [16].

Wide band gap kesterite-type material can open new market opportunities and increase the range of applications. This will tackle two technological applications. First, it can be used for the top cell of cost-efficient tandem photovoltaic devices, and, secondly, for semi-transparent solar cells for advanced concepts of efficient and stable Building Integrated Photovoltaics (BIPV). In the last years, first semi-transparent kesterite-based devices have been successfully produced, achieving efficiencies of 7.9% (CZTSSe with E_g = 1.47 eV) [17] and 5.6% (CZTGSe with E_g = 1.28 eV) [16].

CZGSSe has been shown as a promising candidate to be used for the applications mentioned above, because of its higher band gap energy. In [18], CZGSSe thin films with E_g ranging from 1.5 to 1.7 eV were obtained by controlling the amount of GeS added during the selenization treatment of solution-processed CZGS layers. The increase of the [S]/([S]+[Se]) atomic ratio is responsible for an increased E_g, but the optimization of its distribution through the absorber layer is one of the key challenges for enhancing the device performance. Hironiwa et al. [19] simulated the optimum band gap grading profile of CZTSSe, considering flat, single and double [S]/([S]+[Se]) gradients through the kesterite-type thin film. They concluded that a graded band gap leads to higher efficiencies than a flat distribution of S because of an improved carrier collection. Yang et al. [20] reported a 12.3% CZTSSe-based device achieved by an in-depth S distribution, which consisted of a higher S-content near the surface and a minimum S-content inside the space charge region, resulting in a higher V_{OC} and η. More recently, Lee et al. [21] have also observed that a S-enriched surface makes CZTSSe surface band gap widened and increases V_{OC}.

In this work, the effect of Na on CZGSSe thin films fabricated by sulfurization of co-evaporated CZGSe layers is investigated. The Na content is varied via different thicknesses of a NaF precursor layer deposited before CZGSe co-evaporation. The Na content does not only affect the distribution of S through the absorber layer, but also the band gap energy of the kesterite and the short-circuit current of the final photovoltaic devices. The influence of using a Se capping layer before the sulfurization is also studied.

2. Experimental section

2.1. Deposition of $Cu_2ZnGe(S,Se)_4$ thin films

$Cu_2ZnGe(S,Se)_4$ thin films were fabricated by sulfurization of co-evaporated $Cu_2ZnGeSe_4$ onto Mo/SLG substrates. The co-evaporation of Cu, ZnSe, Ge and Se was performed at a nominal substrate temperature of 150 °C. A first stage consisted of the co-evaporation of all elements together, followed by the co-evaporation of ZnSe, Ge and Se and finishing with a short co-evaporation of Ge and Se [16,22]. Due to the low substrate temperature used and the known beneficial effect of Na on kesterite solar cells [11], a NaF precursor layer was added before the co-evaporation process, varying its thickness from 0 to 15 nm. Before the sulfurization of CZGSe thin films, 500 nm of a Se capping layer was evaporated at room temperature in the same vacuum chamber to protect the samples against possible oxidation and enhance the homogenization during the annealing, as performed in [16,22]. The sulfurization process was carried out at 480 °C for 1 h in Ar atmosphere. The samples, together with elemental S (22 mg) and GeS (5 mg), were placed in a partially closed graphite box and inserted into a tubular furnace. GeS was added to minimize the losses of Ge. The heating rate was set to 20 °C/min and the cooling rate to 10 °C/min [16,21]. In order to investigate the effect of the Se capping layer on the CZGSSe thin films and the resulting solar cells, a deposition process was carried out by using the same growth conditions described above, 15 nm NaF precursor layer and without any Se capping layer.

2.2. Device fabrication

CZGSSe thin films were etched with KCN to clean and remove oxide phases from the absorber surface. After that, a CdS buffer layer of around 50 nm of thickness was grown by chemical bath. A window layer composed of i-ZnO (50 nm) and In_2O_3:SnO_2 (ITO) (350 nm) layers was deposited by DC-pulsed sputtering deposition. Neither grids nor an anti-reflection coating were deposited onto the final photovoltaic devices. In addition to that, no thermal treatment was performed to the solar cells.

2.3. Characterization techniques

Energy dispersive X-ray spectroscopy (EDX) (Oxford instruments, model INCAx-sight) using a Hitachi S-3000N scanning electron microscope (SEM) was used to measure the chemical composition of the kesterite-type thin films. For that, operating voltages of 10 kV and 25 kV and the Cu K, Zn K, Sn L, Ge K, Se K and S K lines were used for elemental quantification. The distribution of elements throughout the thickness of the kesterite absorber layer was measured via glow discharge optical emission spectrometry (GD-OES) using a Spectrum GDA 650. Depth profiles are collected using an Argon plasma in a pulsed RF mode for sputtering and a CCD-array for the optical detection. Measurements were carried out after optimizing the sputtering parameters according to the procedure described in [23]. The measurements were done without calibration samples, which is the reason of showing the depth profiles as qualitative plots. However, these give a reliable representation of the qualitative distribution of the containing elements in the kesterite layers, since all measurements were performed under the very same conditions. The morphology of the CZGSSe/Mo structure was investigated by SEM, using a Philips XL30S FEG SEM, operating at 5 kV.

The structural properties of the CZGSSe thin films were investigated by Grazing incidence X-ray diffraction (GIXRD). A Panalytical X´Pert Pro MPD diffractometer, using CuK_α radiation and a multilayer mirror to produce a parallel beam, were used to collect the GIXRD data. Detector scans with four different incident angles of 0.5°, 1°, 2° and 5° were performed for all of the thin films, in order to collect information from different depths of the absorber (subsurface, bulk and back interface of the absorber). Micro-Raman spectra were recorded using a Horiba's LabRam HR800 spectrometer with a 532 nm laser line to investigate the surface of the CZGSSe absorber layers.

Current-Voltage (*I-V*) characteristics of the photovoltaic devices were measured by using a Sun 3000 class solar simulator (Abet Technologies Inc., Milford, Connecticut, USA) under standard test conditions (25 °C, AM 1.5, 100 mW/cm^2). External quantum efficiency (*EQE*) of the solar cells was measured using a Bentham PVE300 system (Bentham Instruments Ltd., Berkshire, UK) calibrated with a Si and Ge photodiodes.

3. Results and discussion

3.1. Effect of Na content

Table 1 shows the composition of the samples investigated as measured by *EDX* at 10 kV and 25 kV. Higher Cu and Zn concentrations were measured closer to the surface for all the absorber layers, with the exception of the sample without Se capping layer (Sample 5

Table 1
Thickness and composition of $Cu_2ZnGe(S,Se)_4$ thin films measured by EDX. Sample 5 is the only one without Se capping layer.

kV	No.	NaF [nm]	CZGSSe [μm]	[Cu] [%at]	[Zn] [%at]	[Ge] [%at]	[Se] [%at]	[S] [%at]	[Cu]/ ([Zn]+[Ge])	[Zn]/[Ge]	[S]/[VI]	[VI]/[M]
25	1	0	1.36	17.9	13.3	12.4	42.2	18.2	0.69	1.07	0.30	1.38
10				20.0	17.4	10.9	25.7	26.2	0.71	1.65	0.51	1.07
25	2	6	1.31	18.6	11.9	13.9	46.2	9.4	0.72	0.85	0.17	1.25
10				23.4	12.3	12.9	34.3	17.1	0.93	0.95	0.33	1.05
25	3	12	1.33	21.3	11.5	12.7	27.0	28.0	0.88	0.90	0.51	1.21
10				24.3	11.9	12.7	24.9	26.3	0.98	0.94	0.52	1.04
25	4	15	1.00	16.1	14.8	11.9	36.8	20.4	0.61	1.24	0.36	1.34
10				18.0	20.5	9.6	30.2	21.7	0.60	2.15	0.42	1.08
25	5	15	1.40	17.7	13.4	13.1	39.3	16.5	0.67	1.02	0.30	1.30
10				22.6	12.9	12.2	30.9	21.5	0.90	1.06	0.41	1.10

Note: [VI] = [S] + [Se]; [M] = [Cu] + [Zn] + [Ge]

in Table 1). Also, the sulphur concentration is generally higher closer to the surface than in the bulk of the samples, indicating a [S]/([S]+[Se]) gradient through the absorber layer. However, a much more uniform distribution of [S]/([S]+[Se]) atomic ratio is detected for Sample 3 with 12 nm NaF, followed by the sample with thicker NaF layer (Sample 4).

Fig. 1(a)–(d). display the GD-OES depth profiles of the CZGSSe thin films onto which a NaF precursor layer of different thicknesses was evaporated and a Se capping layer was added. There are some common features in most of the samples; namely an accumulation of Ge, a lower Cu and a higher Se-signal near the Mo back contact were detected. A higher S content is also measured at the surface of all the samples. An increased Zn-signal is also observed at the surface of the samples with the exception of the absorber with 12 nm NaF precursor layer. Na diffuses from the back interface towards the absorber surface, increasing the Na-signal inside the kesterite-type film when the thickness of the NaF layer increases. The Na GD-OES signal of Sample 1 corresponds to the Na diffusion from the SLG substrate. Once the NaF thickness is increased to 6 nm (see Fig. 1b), the Na signal is completely altered, and so are the Cu, Ge and Zn depth profiles. A peculiar Na distribution is measured with a significantly increased Na GD-OES signal at around 450 nm from the surface, coinciding with higher Ge and Se contents and lower Cu and Zn concentrations. This behavior demonstrates the known affinity of Na for the Cu vacancies [24]. An increased Ge GD-OES signal is observed near the Mo layer in Sample 2, but much more reduced than that observed for the kesterite absorber without the NaF layer. A single S gradient through the absorber layer is developed, increasing the S content at the same position at which the Na-signal starts to increase (around 450 nm from the surface). When a 12 nm thick NaF precursor layer is evaporated, a rather uniform distribution of S, Se, Ge, and Zn is measured throughout the kesterite film, very different from the rest of the absorber layers, as shown in Fig. 1(c). However, surprisingly, the evaporation of 15 nm NaF precursor layer leads to an accumulation of Ge and Se contents near the Mo back contact as well as to higher Zn and S-GD-OES signals near the surface, similar to the observation made for samples with lower Na concentrations. The CZGSSe absorber layers with 12 and 15 nm NaF precursor layers are characterized by a slight increase of the S signal near the back contact.

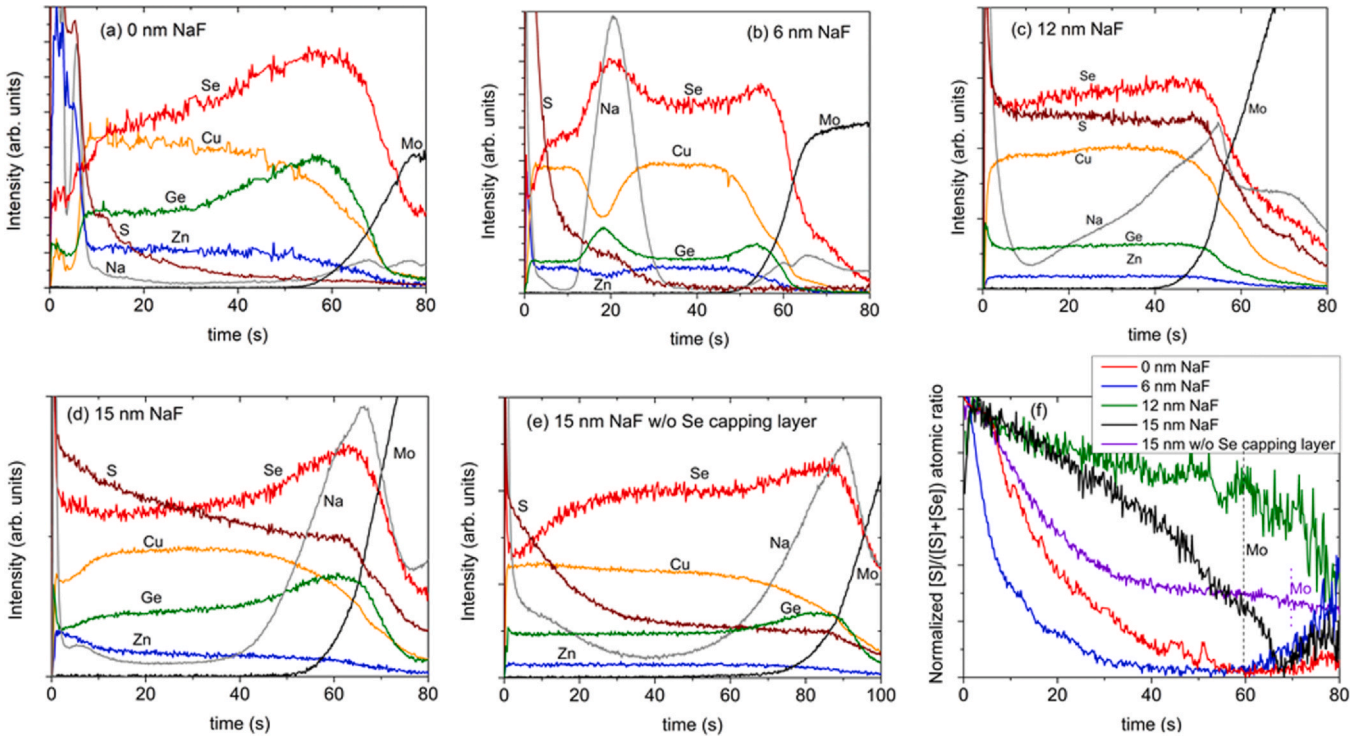

Fig. 1. GD-OES depth profiles of CZGSSe/Mo structure with a Se capping layer before the sulfurization of CZGSe and a NaF precursor layer of (a) 0 nm, (b) 6 nm, (c) 12 nm, (d) 15 nm of thickness. (e) GD-OES depth profiles of CZGSSe/Mo structure with 15 nm NaF and without Se capping layer. (f) Distribution of the normalized [S]/([S]+[Se]) atomic ratio through the absorber layer for all the samples investigated. Dashed and dotted lines are plotted to orientate about the presence of the Mo layer for samples with and without Se capping layer.

As mentioned before, the S and Se-depth profiles, and in consequence, the [S]/([S]+[Se]) gradient through the absorber layer plays an important role to maximize the efficiency of corresponding solar cells [19]. Fig. 1(f) shows the variation of the normalized [S]/([S]+[Se]) atomic ratio through the absorber thickness for all the samples. A similar [S]/([S]+[Se]) depth profile is detected for the samples with 0 and 6 nm NaF, decreasing from the absorber surface towards the back interface, presenting an exponential decay behavior. However, the kesterite thin film with 12 nm NaF precursor layer presents a slighter and continuous increase of the [S]/([S]+[Se]) atomic ratio from the back to the surface of the absorber layer. The CZGSSe layer with the thickest layer of NaF, 15 nm, also presents a continuous increase of the [S]/([S]+[Se]) as in Sample 3, but with a more pronounced slope. All the samples are characterized by a single [S]/([S]+[Se]) gradient through the absorber layer, but with a different evolution depending on the amount of Na, from exponential, up to 6 nm NaF layer, to a polynomial behavior, for thicker NaF layer.

Fig. 2(a)–(d) shows the GIXRD diffraction patterns of the CZGSSe thin films measured with four incidence angles (0.5°, 1°, 2°, and 5°). A sample depth of around 240, 480, 950 and 2500 nm is estimated by using grazing incidence angle of 0.5°, 1°, 2° and 5° respectively. A comparative study like this allows us to get the "depth profile" of the samples. All of the diffraction patterns show Bragg peaks which can be attributed to the kesterite-type structure of CZGSSe, with different [S]/([S]+[Se]) atomic ratios resulting in different lattice constants. The diffraction patterns of the samples with 0 and 6 nm NaF layers, clearly show the presence of two CZGSSe phases with different [S]/([S]+[Se]) ratios, but in all of the cases the Se richer phase stays dominant. A shift to more sulphur-rich compositions towards the surface can be observed in these two samples, which is in a very good agreement with the results of the GD-OES measurements. The *a* and *c* lattice parameters, shown in the Fig. 2(e) and (f), are the result of the LeBail refinement, using kesterite-type structure (space group $I\bar{4}$) as the starting model for refinement. Two CZGSSe phases were included in the refinement for each of the patterns alongside the Mo phase but only the lattice parameter corresponding to the dominant phase is plotted. A decrease in both lattice parameters towards the 0.5° incident angle reflects the change towards the higher [S]/([S]+[Se]) atomic ratio for the dominant CZGSSe phase. The situation changes significantly for the samples with 12 nm and 15 nm NaF. Here, only one CZGSSe phase was used in the refinements. Even though the tendency of slightly S richer

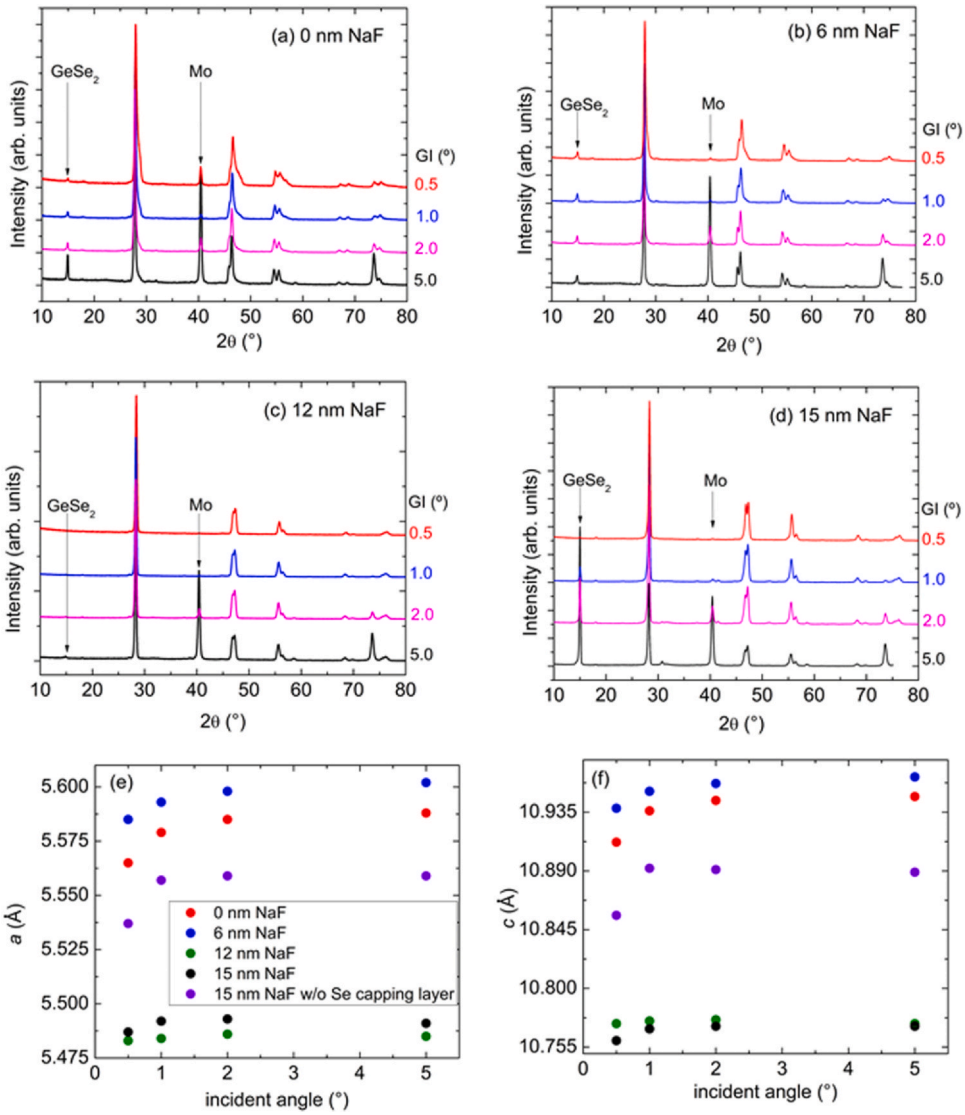

Fig. 2. GIXRD diffraction patterns of CZGSSe absorber layer deposited on Mo/SLG substrate with (a) 0 nm, (b) 6 nm, (c) 12 nm and (d) 15 nm NaF precursor layer and a Se capping layer using incidence angles of 0.5º, 1º, 2º and 5º. Variation of (e) *a* and (f) *c* lattice parameters with the incidence angle obtained by LeBail refinement, using kesterite-type structure (space group $I\bar{4}$) as the starting model for the refinement of all the CZGSSe thin films.

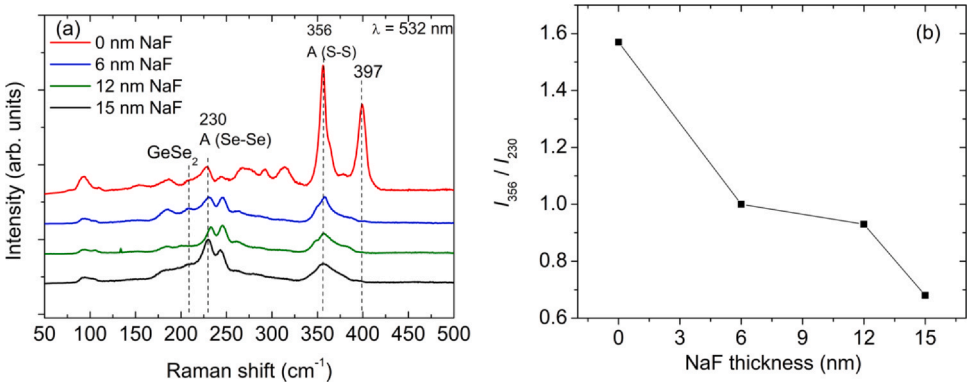

Fig. 3. (a) Raman spectra of CZGSSe absorber layers deposited on Mo/SLG substrate with different thicknesses of the NaF precursor layer and with a Se capping layer. The dominating peaks of CZGSSe are indicated with the dashed lines. (b) Raman peak intensity ratio I_{356}/I_{230} in dependence of the NaF precursor layer thickness in CZGSSe absorber layers. (For interpretation of the references to colour in this figure, the reader is referred to the web version of this article)

composition towards the surface of the film is maintained in these samples as well, the overall drop in the lattice parameters of the samples corresponds to a much S-richer composition, which is in a very good agreement with the values obtained by EDX and shown in Table 1. These results are also in coherence with the different [S]/([S]+[Se])-gradients through the absorber layer as displayed in Fig. 1(f). Therefore, GD-OES and GIXRD measurements show that the development of the [S]/([S]+[Se])-gradient depends on the Na concentration. GIXRD patterns of all the samples are compared for an incidence angle of 1° in Fig. S1 of the Supplementary Material. An increase of the S content for samples with higher Na concentrations, 12 and 15 nm NaF (see Fig. S1) is observed, as mentioned above. The refinements of the absorber layer with 6 nm NaF for a grazing incidence angle of 2° is shown in Fig. S2, as an example.

Apart from the kesterite-type phase, $GeSe_2$ as secondary phase was detected in all of the samples (see Fig. 2a–d). The behavior of this phase differs very much from sample to sample. There is a clear depth distribution, with agglomeration of this phase at the back contact for the Samples 1 and 4 (it can be clearly observed in Fig. 2(a) and (d)). For the Sample 2, the distribution of this phase through the sample is almost uniform, while for Sample 3, this phase is only hardly noticeable in the 5° incident angle measurement, at the back contact. All of these seem to be in a rather good agreement with the Ge and Se profiles of the GD-OES, where Sample 3 (12 nm NaF) is the one with the most homogeneous distribution of Ge throughout the thin film.

GD-OES depth profiles and GIXRD analysis have indicated that Na promotes the diffusion of S towards the bulk of the CZGSe thin films. In general, a certain Na concentration near the Mo back contact seems to be necessary to incorporate S in the bulk of the absorber layer. The same behavior was observed during the sulfurization of CZTSe thin films using ceramic and SLG substrates [15]. As shown in Table 1, the [Cu]/([Zn] + [Ge]) and [Zn]/[Ge] atomic ratios are not the same for all the samples. Therefore, we cannot rule out that those different ratios could affect the [S]/([S]+[Se]) distribution through the CZGSSe layer. However, those cationic ratios have been obtained by the only variation of the thickness of the NaF layer without modifying any other growth process parameter.

As it has been already shown, a clear [S]/([S]+[Se])-gradient with a higher S content near the surface of all the CZGSSe thin films has been determined by GD-OES and GIXRD measurements. The accumulation of S near the surface can be a key parameter to increase the device performance, mainly due to a higher V_{OC}. In order to shed light to the composition at the surface of the absorber layers, Raman spectroscopy measurements were carried out using 532 nm excitation wavelength. Fig. 3(a) shows the Raman spectra of the CZGSSe films with different NaF precursor layer thicknesses. The main modes corresponding to the kesterite-type CZGSSe phase showing bi-modal behavior are detected for all the samples, the dominating A symmetry modes positioned at 230 cm^{-1} (related to Se–Se vibrations in CZGSSe) and 356 cm^{-1} (related to the S–S vibrations in CZGSSe) [18,25]. In addition, the Raman peak at around 210 cm^{-1} could correspond to the $GeSe_2$ secondary phase [26]. That Raman mode could also correspond to the kesterite phase; however, the presence of $GeSe_2$ gains strength as it has been identified by GIXRD measurements (see Fig. 2). Furthermore, that mode at around 210 cm^{-1} is not detected for Sample 3, in agreement with GIXRD diffraction patterns in which $GeSe_2$ was only observed near the back contact. A clear dependence of the intensity of the Raman mode at around 356 cm^{-1} with the NaF thickness is observed. Fig. 3(b) displays the intensity ratio of the dominating Raman modes at 356 cm^{-1} and 230 cm^{-1}, I_{356}/I_{230}, in dependence of the NaF precursor layer thickness. One can see from Fig. 3(b) that the I_{356}/I_{230} ratio is decreasing with the increase in the Na concentration which indicates the decrease in the sulphur concentration at the surface. As detected by GD-OES and GIXRD measurements, a higher accumulation of sulphur near the surface with respect to the bulk of the absorber occurs for samples with lower Na concentrations. Moreover, in addition to the intensity ratio I_{356}/I_{230}, the intensity of the Raman peak at around 397 cm^{-1} can be correlated with the [S]/([S]+[Se])-atomic ratio as can be seen from Fig. 3(a). Using a green excitation wavelength of 532 nm as in these Raman measurements creates close to resonance conditions for the pure CZGS compound influencing the sulphur related E/B symmetry modes (like the mode at around 397 cm^{-1}) [25,27]. The higher the [S]/([S]+[Se])-atomic ratio, the closer is the band gap of the CZGSSe solid solutions to the resonant conditions resulting in the increased intensity of the Raman peak at around 397 cm^{-1}. Then, a higher band gap energy is expected for the CZGSSe without NaF precursor layer. Raman spectroscopy allows us to confirm the influence of Na content on the S concentration accumulated near the surface of CZGSSe layers.

Fig. 4 displays the cross-sectional SEM images of the CZGSSe/Mo structure using the different absorber layers, showing a dense and pinhole-free absorber morphology. Larger grain sizes are observed for samples with a NaF precursor layer with the exception of the Sample 2 with 6 nm of NaF, which could be related to its lower S concentration, as measured by EDX and confirmed by GIXRD. Very large grains of the kesterite-type semiconductor are detected for absorber layers with higher Na content. It can be also distinguished a very thin layer of smaller grain sizes at the surface of some absorber layers, especially for the sample without and with 15 nm NaF [11]. Both samples are characterized by a high Zn content, as measured by EDX at 10 kV, which could be related to the formation of a Zn(S,Se) or ZnS secondary phase. This phase cannot be detected by GIXRD

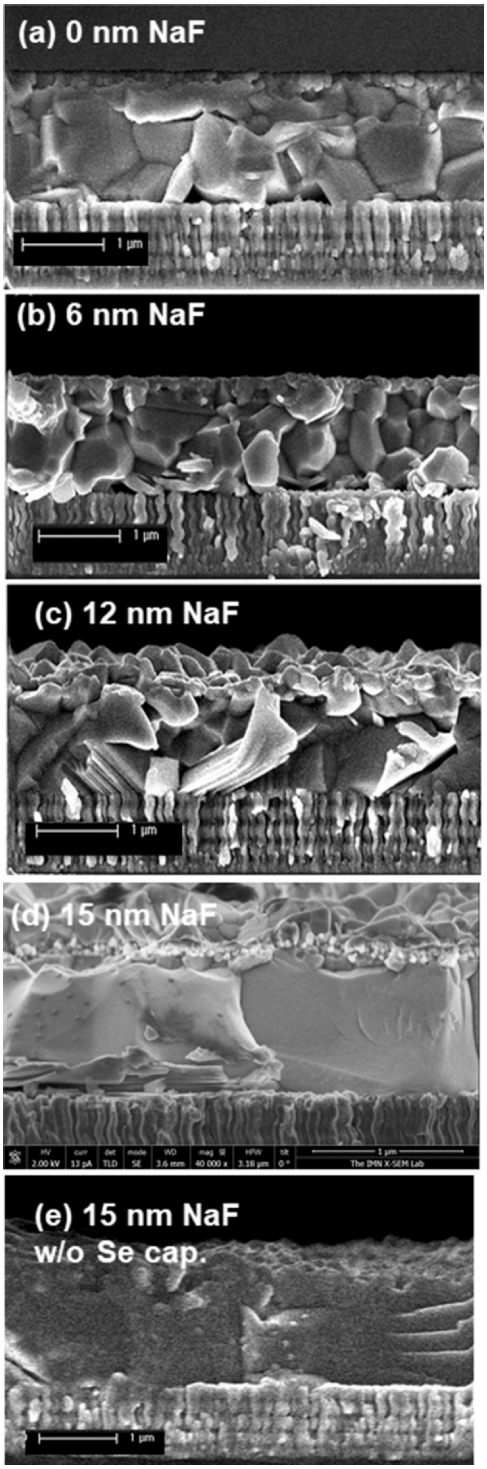

Fig. 4. Cross-sectional SEM pictures of CZGSSe/Mo structure of all the samples investigated.

measurements because the ZnS Bragg peaks (ICDD number: 01–071–59769) overlap with those of CZGSSe.

Fig. 5(a) shows the *EQE* spectra of the best solar cells using the different NaF precursor layers. The integrated short circuit current density J_{SC} was calculated from *EQE* measurements (see Fig. 5a). The less Na is added, the lower the *EQE* is in the whole range of wavelengths, explaining the lower J_{SC}. The average optical band gap energy was determined from the *EQE* spectra. The peak energy of the derivative (or inflection point) of the *EQE* curve can be interpreted as the average band gap energy of the absorber layer. It has been reported that the derivative method, d*EQE*/d*E*, gives results in best agreement with absorption measurements [28]. The variation of E_g with the NaF thickness is plotted in Fig. 5(b). For the lowest Na concentration, the sample without NaF layer, a band gap energy of 2.21 eV is obtained. The addition of a NaF precursor layer decreases E_g, achieving a plateau at around 1.83 eV starting at 6 nm NaF precursor layer. A slightly increase of E_g up to 1.84 eV is observed again when adding 15 nm NaF precursor layer. The samples with 12 and 15 nm NaF present smaller lattice parameters due to a higher S incorporation into the bulk of CZGSe layers (see Fig. 2e and f). However, lower band gap energies are achieved for those thin films in comparison to the one with the lowest Na concentration. Thus, the sample without NaF layer presents the highest E_g and the higher S accumulation at the surface region, as determined by Raman spectroscopy. This emphasizes the importance of the S-gradient developed through the absorber layer, that allows for higher E_g when more S is accumulated at the surface despite a lower S content in the bulk of the CZGSSe layer. A similar effect was observed in CIGSSe thin-film solar cells, in which a higher S content did not lead to a higher band gap energy of CIGSSe. Part of the sulphur was not actually incorporated into the crystal but accumulating at grain boundaries and defects, as observed by Transmission Electron Microscopy (TEM) investigation [29].

Table 2 shows the photovoltaic parameters of the best solar cells represented in Fig. 5. The integrated J_{SC} determined by *EQE* measurements is presented in brackets as well as the efficiency calculated using this integrated value (active area). As it is observed, the integrated J_{SC} is lower than that obtained from *J-V* curve analysis for the samples with a Se capping layer, especially for Devices 2 and 3. Becerril-Romero et al. [17] claim that this behavior indicates the presence of charged defects that affect collection during low-light-intensity *EQE* measurements, but are partially neutralized by photogenerated carriers under more intense illumination in *J-V* curve acquisition. From here on, we will consider the active area-efficiency of the devices. Generally, an enhanced V_{OC} for higher Na concentrations has been reported [11]; however, here no tendency in V_{OC} with the Na content can be found. It should be taken into account that $GeSe_2$ secondary phases are present in the absorber layers, as well as the presence of Zn(S,Se) near the surface of some of the samples cannot be ruled out in view of the EDX and GD-OES results, which can be detrimental for V_{OC} [16]. In addition, the different S-gradient and S contents are fundamental factors for the enhancement of V_{OC}. Sample 1 without NaF precursor layer presents a V_{OC} = 756 mV and it is the absorber layer characterized by the highest S content on the surface as determined by Raman spectroscopy. The high increase of Zn near the surface region (see Fig. 1a) and the inhomogeneous in-depth distribution of the elements could be responsible for the low device performance. Sample 3 with 12 nm NaF precursor layer was characterized by a very uniform distribution of S throughout the CZGSSe layer as detected by GD-OES and the uniform in-depth distribution of the lattice parameters; however, only a 1.8% efficiency was achieved. Despite the higher S concentration measured by EDX, the lowest V_{OC} is obtained. As reported by Hironiwa et al. [19], a flat distribution of S throughout a CZTSSe film resulted in lower performance than the development of a graded band gap obtained via a gradient of the S distribution.

However, there is a relationship between the Na content and J_{SC} and fill factor, *FF,* values. A higher Na concentration results in an improved carrier collection, which leads to a higher J_{SC}, as well as in higher *FF*, leading to better devices. The highest efficiency of 2.8%, mainly due to a higher V_{OC} and *FF*, is achieved for the CZGSSe thin film with the thickest NaF layer and E_g = 1.84 eV. The better *FF* values obtained for the devices with 12 nm and 15 nm NaF could be related to an enhanced CZGSSe/Mo back interface. As mentioned above, not only a higher Se concentration was detected near the Mo layer, but also a slight increase of S for absorber layers with 12 and 15 nm NaF

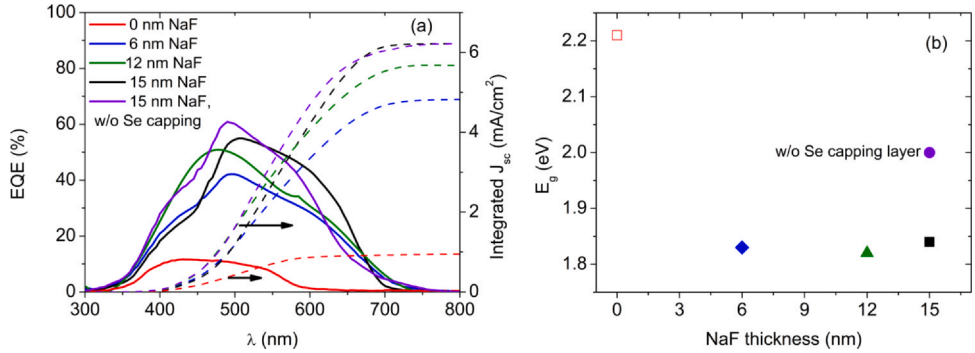

Fig. 5. (a) *EQE* spectra and integrated J_{SC} of the best devices of all samples investigated. (b) Variation of the band gap energy E_g of the different CZGSSe absorber layers versus the thickness of the NaF layer.

Table 2
PV parameters of the different CZGSSe photovoltaic devices investigated.

Sample	Se capping layer	NaF (nm)	V_{OC} (mV)	J_{SC} (mA/cm^2)	*FF* (%)	η (%)
1	Yes	0	756	1.3 (1.0)	43.8	0.4 (0.3)
2	Yes	6	642	7.9 (4.8)	48.0	2.5 (1.5)
3	Yes	12	631	14.4 (5.7)	50.0	4.6 (1.8)
4	Yes	15	793	6.6 (6.2)	56.3	3.0 (2.8)
5	No	15	828	5.4 (6.2)	52.0	2.3 (2.7)

(see Fig. 1), could be an indication of the formation of a thin Mo $(S,Se)_2$ layer between the absorber and back contact that allows for enhancing that interface. As shown in Fig. 2(d) for the sample with 15 nm NaF precursor layer, the intensity of that Bragg peak increases when the incidence angle increases. The sample with 12 nm NaF presents this Bragg peak only near the back contact. It is known that Na acts as a catalyst that promotes the formation of $MoSe_2$ at the CIGSe/Mo interface [30], and something similar could occur here with S and Se when more Na is added. Further investigations are necessary to be able to conclude about this aspect.

Therefore, it has been demonstrated that the Na content is a key parameter to control the sulfurization process of the CZGSe thin films, as observed previously by de la Cueva et al. [15] for CZTSSe, which influences not only the structural and compositional properties of the absorber layer, but also its band gap energy and the device performance.

3.2. Effect of the Se capping layer

In previous works, a Se capping layer was evaporated before the thermal treatment in the case of CZTGSe thin films [16,22]. This capping layer was used to enhance the homogeneity during the annealing, reduce elemental losses and protect the absorber surface of possible oxidation. However, when the annealing is performed in the presence of another new element as S, the Se capping layer does not play the role of homogenization, as detected by GD-OES depth profiles (see Fig. 1). In view of these results, a new experiment was designed to investigate the influence of the Se capping layer on the CZGSSe thin films and final devices. In this experiment, no Se capping layer was evaporated after the CZGSe co-evaporation process and a 15 nm thick NaF precursor layer was deposited because of the highest solar cell efficiency obtained by using this thickness. Table 1 shows the composition of this Sample 5 without Se capping layer. A lower sulphur content was incorporated in the bulk of the absorber layer. Fig. 1(e) displays the GD-OES depth profile of the elements through the CZGSSe layer grown without the Se capping layer. The main difference between this sample and the Sample 4 (see Fig. 1d) occurs near the surface. The absorber layer with the Se capping layer, Sample 4, presents a drop of the Ge and Cu-signals and an increased Zn concentration at the surface, while the sample without the capping layer is characterized by a more uniform distribution of the cations near the surface. Furthermore, the distribution of S and Se are different, as it is revealed in Fig. 1(e) and (f). Now, the [S]/([S]+[Se])-gradient of the sample without Se capping layer is similar to those observed for lower Na concentrations, but with a higher S concentration in the bulk of the absorber layer.

Fig. 6(a) shows the diffraction patterns of Sample 5 using different incident angles. Kesterite-type, Mo and $GeSe_2$ phases are identified, as in the other samples investigated. An accumulation of $GeSe_2$ in the back region of the absorber layer is detected in agreement with the GD-OES results. Fig. 6(b) displays the 112 Bragg peak of Samples 4 and 5 for incident angles of 0.5°, 1°, 2° and 5°. A higher S content near the surface is detected in both samples, in agreement with EDX measurements and GD-OES depth profiles. As mentioned above, only one CZGSSe phase was necessary for the refinement of the diffraction patterns of Sample 4; however, it is clearly observed that two phases with different S content are necessary for Sample 5. In addition to that, a higher S content in the bulk of the absorber layer is confirmed for the sample with the Se capping layer. Fig. 2(e) and (f) display the *a* and *c* lattice parameters of Sample 5 without Se capping layer, presenting a similar variation of *a* and *c* with the incident angles to that determined for the CZGSSe with lower Na concentration in agreement with GD-OES profiles. In order to confirm the higher accumulation of S on the surface for the absorber layer without Se capping layer, Raman spectroscopy was performed, as shown in Fig. 6(c). As observed, a completely different Raman spectrum is measured for the sample without Se capping layer. The shift of the Raman peaks towards higher wavenumbers and the double peak structure of the CZGS peak at around 355 cm^{-1} (352 and 360 cm^{-1}) indicates a higher sulphur content in this sample [27]. In addition, the high intensity of the peak at 392 cm^{-1} supports this, similar to the mode at around 397 cm^{-1} for the sample without NaF precursor layer.

It could happen that the Se capping layer can hinder the S incorporation at the surface in the beginning of the thermal process, then the diffusion and replacement of Se by S take place during the sulfurization process at 480 °C. This results in a higher S concentration in the bulk of the absorber film and the S-grading decreasing from surface to the back of the CZGSSe layer. Further investigations are necessary to understand the role of the Se capping layer on the growth kinetic of CZGSSe.

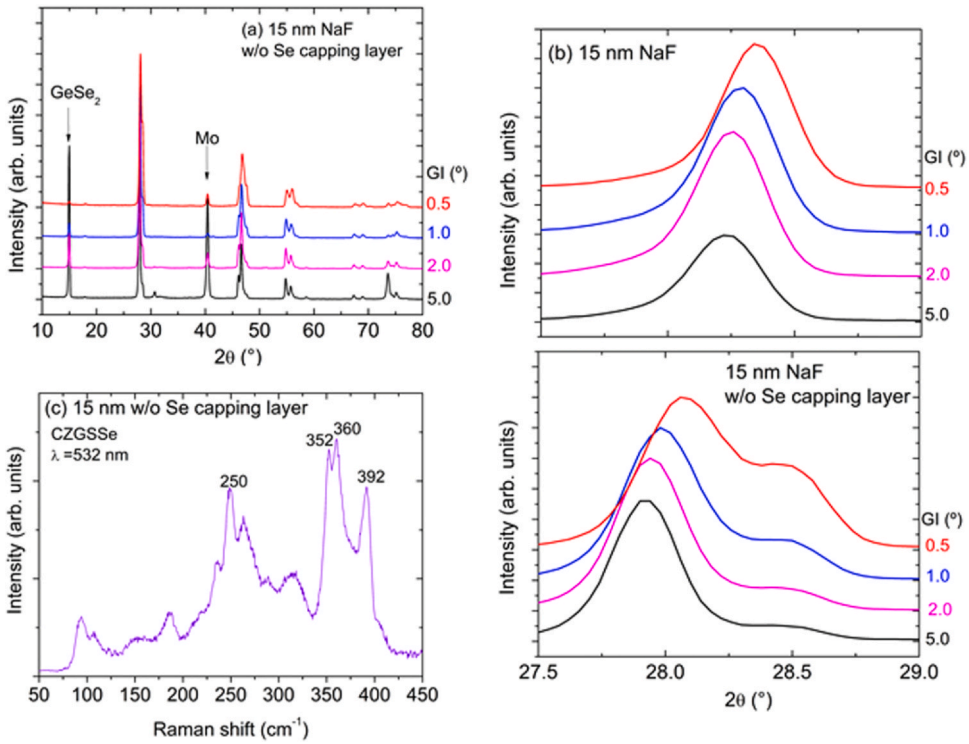

Fig. 6. (a) GIXRD patterns of sample 5 without Se capping layer using different incident angles. (b) 112 Bragg peak of CZGSSe absorber layers with 15 nm NaF, with and without Se capping layer for grazing incidence angles of 0.5º, 1º, 2º and 5º. (c) Raman spectrum of CZGSSe with 15 nm NaF and without Se capping layer measured using 532 nm excitation wavelength.

Cross-sectional SEM images of the CZGSSe/Mo structure using Sample 5 are shown in Fig. 4.e). This is characterized by a compact structure with large kesterite grain size. In comparison with Sample 4, it is not possible to distinguish any thin layer at the surface for Sample 5 in agreement with a more uniform distribution of the cations in this region, as detected by GD-OES measurements.

A band gap energy of 2.0 e V was determined from *EQE* of Device 5 with an efficiency (active area) of 2.7% (see Fig. 5 and Table 2). The evaporation of 15 nm NaF precursor layer led to the same J_{SC} independent from the presence or absence of the capping layer. However, a higher V_{OC} of 828 mV is achieved for the absorber without Se capping layer. The increased V_{OC} can be due to different factors, such as the uniform distribution of the cations near the surface no expecting ZnS secondary phase, and the distribution of S through the absorber layer. As mentioned above, the CZGSSe absorber layer without Se capping film presents some similar characteristics to the sample with lowest Na concentration, as the [S]/([S]+[Se]) depth profile but with a higher S concentration in the bulk of CZGSSe, which can be the key factor to enhance V_{OC} and control the E_g of the absorber. The efficiency of 2.7% of the Device 5 is limited by a *FF* lower than that of Device 4.

For the first time, the importance of the Na content and a Se capping layer to modify the [S]/([S]+[Se])-gradient and the band gap energy of the kesterite absorber layer has been demonstrated. The next challenge is to develop a way to increase E_g maintaining a high efficiency. In addition, the knowledge obtained here can be transfer towards designing devices with transparent back contacts for stable semi-transparent solar cells.

4. Conclusion

CZGSSe thin films have been fabricated by sulfurization of co-evaporated CZGSe. The effect of a NaF precursor layer and the presence of a Se capping layer before the sulfurization process have been investigated. The dependence of CZGSSe properties on the addition of Na via a NaF layer, with thickness from 0 to 15 nm, when a Se capping layer was evaporated, has been demonstrated:

1. A higher S concentration was detected near the surface independent from the Na content added, as investigated by GD-OES and GIXRD measurements. However, the S distribution depended on the thickness of the NaF layer, distinguishing different behaviors for samples between 0 and 6 nm NaF and those with 12–15 nm NaF layer.
2. A band gap energy of 2.21 eV was achieved for CZGSSe absorber layer without NaF. From 6 nm NaF, E_g was maintained in the range of 1.83 eV. The much higher E_g for the NaF-free sample may be related to the much higher accumulation of S at the surface, as determined by Raman spectroscopy.
3. A uniform S-depth profile does not lead to better solar cells and also, not necessarily to higher band gap energies, as observed for the Sample with 12 nm NaF.
4. A relationship between the Na added and the J_{SC} and *FF* values of the final solar cells was found: higher Na contents lead to higher J_{SC} and *FF*. Thicker NaF layer of 15 nm resulted in higher efficiencies of 2.8%.

The suppression of the Se capping layer is investigated on the CZGSSe properties when 15 nm NaF precursor layer was added. This allows for a higher accumulation of S near the surface, achieving an efficiency of 2.7%, V_{OC} of 828 mV and E_g = 2.0 eV.

CRediT authorship contribution statement

Andrea Ruiz-Perona: Investigation, Fabrication of CZGSSe absorber layers by co-evaporation and sulfurization process, Investigation, Discussion. **Michael Sun:** Investigation, Fabrication of CZGSSe absorber layers by co-evaporation and sulfurization process, Investigation, Discussion. **Galina Gurieva:** GIXRD measurements, Data analysis, Writing about GIXRD results and Discussion, Data

curation, Formal analysis, Writing. **Tim Kodalle:** GD-OES measurements, review & editing, Discussion, Data curation, Resources. **Yudania Sánchez:** Finalization of solar cells, I-V and EQE measurements, Methodology, Resources. **Maarja Grossberg:** Raman measurements, Data analysis, Writing about Raman results and Discussion, Data curation, Formal analysis, Writing. **José Manuel Merino:** Funding acquisition, Writing - review & editing. **Susan Schorr:** Supervision of GIXRD results, Writing - review & editing. **Máximo León:** Discussion. **Raquel Caballero:** Conceptualization, Investigation, Supervision, Designing of experiments, Writing - original draft, Writing - review & editing, Funding acquisition.

Declaration of Competing Interest

The authors declare that they have no known competing financial interests or personal relationships that could have appeared to influence the work reported in this paper.

Acknowledgements

This work was supported by Spanish Ministry of Science and Innovation Project WINCOST (ENE2016-80788-C5–2-R), CELL2WIN (PID2019-104372RB-C32) and European Project INFINITE-CELL (H2020-MSCA-RISE-2017–777968). ARP also acknowledges financial support from Community of Madrid within Youth Employment Program (PEJD-2017-PRE/IND-4062). M.G. also acknowledges financial support from L′Oréal Baltic For Women in Science Programme and from the European Regional Development (Project TK141). The authors would like to thank K. Mayer-Stillrich and M. Hartig at PVComB-HZB for Mo deposition.

Appendix A. Supporting information

Supplementary data associated with this article can be found in the online version at doi:10.1016/j.jallcom.2021.159253.

References

[1] W. Wang, M.T. Winkler, O. Gunawan, T. Gokmen, T.K. Todorov, Y. Zhu, D.B. Mitzi, Device characteristics of CZTSSe thin-film solar cells with 12.6% efficiency, Adv. Energy Mater. 4 (2014) 1301465, https://doi.org/10.1002/aenm.201301465

[2] D.H. Son, S.H. Kim, S.Y. Kim, Y.I. Kim, J.H. Sim, S.N. Park, D.H. Jeon, D.K. Hwang, S.J. Sung, J.K. Kang, K.J. Yang, D.H. Kim, Effect of solid-H_2S gas reactions on CZTSSe thin film growth and photovoltaic properties of a 12.62% efficiency device, J. Mater. Chem. A 7 (2019) 25279–25289, https://doi.org/10.1039/C9TA08310C

[3] M.A. Green, E.D. Dunlop, J. Honl-Ebinger, M. Yoshita, N. Kopidakis, X. Hao, Solar cell efficiency tables (version 56), Prog. Photovolt. Res. Appl. 28 (2020) 629–638, https://doi.org/10.1002/pip.3303

[4] T.J. Huang, X. Yin, G. Qi, H. Gong, CZTS-based materials and interfaces and their effects on the performance of thin film solar cells, Phys. Status Solidi RRL 8 (2014) 735–762, https://doi.org/10.1002/pssr.201409219

[5] S. Kim, K.M. Kim, H. Tampo, H. Shibata, S. Niki, Improvement of voltage deficit of Ge-incorporated kesterite solar cell with 12.3% conversion efficiency, Appl. Phys. Express 9 (2016) 102301, https://doi.org/10.7567/APEX.9.102301

[6] S. Kim, K.M. Kim, H. Tampo, H. Shibata, K. Matsubara, S. Niki, Ge-incorporated $Cu_2ZnSnSe_4$ thin-film solar cells with efficiency greater than 10%, Sol. Energy Mater. Sol. Cells 144 (2016) 488–492, https://doi.org/10.1016/j.solmat.2015.09.039

[7] E. Garcia-Llamas, J.M. Merino, R. Serna, X. Fontané, I.A. Victorov, A. Pérez-Rodríguez, M. León, I.V. Bodnar, V. Izquierdo-Roca, R. Caballero, Wide band-gap tuning $Cu_2ZnSn_{1-x}Ge_xS_4$ single crystals: optical and vibrational properties, Sol. Energy Mater. Sol. Cells 158 (2016) 147–153, https://doi.org/10.1016/j.solmat.2015.12.021

[8] M. Neuschitzer, J. Márquez, S. Giraldo, M. Dimitrievska, M. Placidi, I. Forbes, V. Izquierdo-Roca, A. Pérez-Rodríguez, E. Saucedo, V_{oc} boosting and grain growth enhancing Ge-doping strategy for $Cu_2ZnSnSe_4$ photovoltaic absorbers, J. Phys. Chem. C 120 (2016) 9661–9670, https://doi.org/10.1021/acs.jpcc.6b02315

[9] A.D. Collord, H.W. Hillhouse, Germanium alloyed kesterite solar cells with low voltage deficits, Chem. Mater. 28 (2016) 2067–2073, https://doi.org/10.1021/acs.chemmater.5b04806

[10] L. Choubrac, M. Bär, X. Kozina, R. Félix, R.G. Wilks, G. Brammertz, S. Levcenko, L. Arzel, N. Barreau, S. Harel, M. Meuris, B. Vermang, Sn substitution by Ge: strategies to overcome the open-circuit voltage deficit of kesterite solar cells, Appl. Energy Mater. 3 (6) (2020) 5830–5839, https://doi.org/10.1021/acsaem.0c00763

[11] Y.E. Romanyuk, S.G. Haass, S. Giraldo, M. Placidi, D. Tiwari, D.J. Fermin, X. Hao, H. Xin, T. Schnabel, M. Kauk-Kuusik, P. Pistor, S. Lie, L.H. Wong, Doping and alloying of kesterites, J. Phys. Energy 1 (2019) 044004, https://doi.org/10.1088/2515-7655/ab23bc

[12] S.G. Haass, C. Andres, R. Figi, C. Schreiner, M. Bürki, Y.E. Romanyuk, A.N. Tiwari, Complex interplay between absorber composition and alkali doping in high--efficiency kesterite solar cells, Adv. Energy Mater. 8 (4) (2018) 1701760, https://doi.org/10.1002/aenm.201701760

[13] A. Cabas-Vidani, S.G. Haass, C. Andres, R. Caballero, R. Figi, C. Schreiner, J.A. Márquez, C. Hages, T. Unold, D. Bleiner, A.N. Tiwari, Y.E. Romanyuk, High-efficiency $(Li_xCu_{1-x})_2ZnSn(S,Se)_4$ kesterite solar cells with lithium alloying, Adv. Energy Mater. 8 (34) (2018) 1801191, https://doi.org/10.1002/aenm.201801191

[14] H. Xie, S. López-Marino, T. Olar, Y. Sánchez, M. Neuschitzer, F. Oliva, S. Giraldo, V. Izquierdo-Roca, I. Lauermann, A. Pérez-Rodríguez, E. Saucedo, Impact of Na dynamics at the $Cu_2ZnSn(S,Se)_4$/CdS interface during post low temperature treatment of absorbers, Appl. Mater. Interfaces 8 (7) (2016) 5017–5024, https://doi.org/10.1021/acsami.5b12243

[15] L. de la Cueva, Y. Sánchez, L. Calvo-Barrio, V. Izquierdo-Roca, S. Khelifi, T. Bertram, J.M. Merino, M. León, R. Caballero, Sulfurization of co-evaporated $Cu_2ZnSnSe_4$ thin film solar cells: the role of Na, Sol. Energy Mater. Sol. Cells 186 (2018) 115–123, https://doi.org/10.1016/j.solmat.2018.06.015

[16] A. Ruiz-Perona, Y. Sánchez, M. Guc, S. Khelifi, T. Kodalle, M. Placidi, J.M. Merino, M. León, R. Caballero, Effect of Na and the back contact on $Cu_2Zn(Sn,Ge)Se_4$ thin-film solar cells: towards semi-transparent solar cells, Sol. Energy 206 (2020) 555–563, https://doi.org/10.1016/j.solener.2020.06.044

[17] I. Becerril-Romero, D. Sylla, M. Placidi, Y. Sánchez, J. Andrade-Arvizu, V. Izquierdo-Roca, M. Guc, A. Pérez-Rodríguez, S. Grini, L. Vines, B. Pusay, R. Almache, J. Puigdollers, P. Pistor, E. Saucedo, M. Espíndola-Rodríguez, Transition-metal oxides for kesterite solar cells developed on transparent substrates, ACS Appl. Mater. Interfaces 12 (2020) 33656–33669, https://doi.org/10.1021/acsami.0c06992

[18] T. Schnabel, M. Seboui, E. Ahlswede, Band gap tuning of $Cu_2ZnGeS_xSe_{4-x}$ absorbers for thin-film solar cells, Energies 10 (2017) 1813, https://doi.org/10.3390/en10111813

[19] D. Hironiwa, M. Murata, N. Ashida, Z. Tang, T. Minemoto, Simulation of optimum band-gap grading profile of $Cu_2ZnSn(S,Se)_4$ solar cells with different optical and defect properties, Jpn. J. Appl. Phys. 53 (7) (2014) 071201, https://doi.org/10.7567/JJAP.53.071201

[20] K.J. Yang, D.H. Son, S.J. Sung, J.H. Sim, Y.I. Kim, S.N. Park, D.H. Jeon, J. Kim, D.K. Hwang, C.W. Jeon, D. Nam, H. Cheong, J.K. Kang, D.H. Kim, A band-gap-graded CZTSSe solar cell with 12.3% efficiency, J. Mater. Chem. A 4 (2016) 10151–10158, https://doi.org/10.1039/C6TA01558A

[21] J. Lee, T. Enkhbat, G. Han, M.H. Sharif, E. Enkhbayar, H. Yoo, J.H. Kim, S. Kim, J. Kim, Over 11% efficient eco-friendly kesterite solar cell: effects of S-enriched surface of $Cu_2ZnSn(S,Se)_4$ absorber and band gap controlled (Zn,Sn)O buffer, Nano Energy 78 (2020) 105206, https://doi.org/10.1016/j.nanoen.2020.105206

[22] A. Ruiz-Perona, Y. Sánchez, M. Guc, L. Calvo-Barrio, T. Jawhari, J.M. Merino, M. León, R. Caballero, Influence of Zn excess on compositional, structural and vibrational properties of $Cu_2ZnSn_{0.5}Ge_{0.5}Se_4$ thin films and their effect on solar cell efficiency, Sol. Energy 199 (2020) 864–871, https://doi.org/10.1016/j.solener.2020.02.082

[23] T. Kodalle, D. Greiner, V. Brackmann, K. Prietzel, A. Scheu, T. Bertram, P. Reyes-Figueroa, T. Unold, D. Abou-Ras, R. Schaltmann, C.A. Kaufmann, V. Hoffmann, Glow discharge optical emission spectrometry for quantitative depth profiling of CIGS thin-films, J. Anal. Spectrom. 34 (2019) 1233–1241, https://doi.org/10.1039/C9JA00075E

[24] R. Caballero, C.A. Kaufmann, V. Efimova, T. Rissom, V. Hoffmann, H.W. Schock, Investigation of Cu(In,Ga)Se2thin-film formation during the multi-stage co-evaporation process: CIGSe thin-film formation multi-stage co-evaporation process, Prog. Photovolt.: Res. Appl. 21 (2013) 30–46, https://doi.org/10.1002/pip.1233

[25] E. Garcia-Llamas, M. Guc, I.V. Bodnar, X. Fontané, R. Caballero, J.M. Merino, M. León, V. Izquierdo-Roca, Multiwavelength excitation Raman scattering of $Cu_2ZnSn_{1-x}Ge_x(S,Se)_4$ single crystals for earth abundant photovoltaic applications, J. Alloy. Compd. 692 (2017) 249–256, https://doi.org/10.1016/j.jallcom.2016.09.035

[26] Z.V. Popović, Z. Jakšić, Y.S. Raptis, E. Anastassakis, High-pressure Raman-scattering study of germanium diselenide, Phys. Rev. B 57 (1998) 3418–3422, https://doi.org/10.1103/PhysRevB.57.3418

[27] M. Guc, M. Neuschitzer, D. Hariskos, A. Bauer, W. Witte, W. Hempel, L. Calvo-Barrio, P. Pistor, A. Pérez-Rodríguez, V. Izquierdo-Roca, Raman scattering quantitative assessment of the anion composition ratio in Zn(O,S) layers for Cd-free chalcogenide-based solar cells, RSC Adv. 6 (2016) 24536–24542, https://doi.org/10.1039/C5RA26261E

[28] R. Carron, C. Andres, E. Avancini, T. Feurer, S. Nishiwaki, S. Pisoni, F. Fu, M. Lingg, Y.E. Romanyuk, S. Bucheler, A.N. Tiwari, Bandgap of thin film solar cell absorbers: a comparison of various determination methods, Thin Solid Films 669 (2019) 482–486, https://doi.org/10.1016/j.tsf.2018.11.017

[29] T. Kodalle, S.S. Schmidt, C. Wolf, D. Greiner, U. Bloeck, P. Schubert-Bischoff, C.A. Kaufmann, R. Schlatmann, Investigating sulfur distribution and corresponding bandgap grading in $Cu(In,Ga)(S,Se)_2$ absorber layers processed by fast atmospheric chalcogenization of metal precursors, J. Alloy. Compd. 703 (2017) 600–604, https://doi.org/10.1016/j.jallcom.2017.01.329

[30] R. Caballero, M. Nichterwitz, A. Steigert, A. Eicke, I. Lauermann, H.W. Schock, C.A. Kaufmann, Impact of Na on $MoSe_2$ formation at the CIGSe/Mo interface in thin-film solar cells on polyimide foil at low process temperatures, Acta Mater. 63 (2014) 54–62, https://doi.org/10.1016/j.actamat.2013.09.051